中北大学学报(自然科学版)
JOURNAL OF NORTH UNIVERSITY OF CHINA(NATURAL SCIENCE EDITION)
2026年 第47卷 第3期(总第227期)
Vol. 47 No. 3 2026(Sum No. 227)

文章编号：1673-3193(2026)03-0315-14 J. North Univ. China, Nat. Sci. Ed., 2026, 47(3): 315-328.

钴/铬共掺杂协同增强NiS的尿素电氧化性能

贾卓榕[1,2]，张雨娟[1,2]，胡拖平[1,2*]

(1. 中北大学 化学与化工学院， 山西 太原 030051；
2. 中北大学 氢能炭基电极材料山西省重点实验室，山西 太原 030051)

摘　要：在尿素氧化反应(UOR)辅助电解水制氢过程中，构筑用于UOR的高性能镍基催化剂是提高制氢效率的关键问题。本文采用水热-煅烧法，在碳布(CC)上制备了钴/铬共掺杂的硫化镍复合物(Co,Cr-NiS/CC)。通过X射线衍射(XRD)、扫描电子显微镜(SEM)、透射电子显微镜(TEM)、X射线光电子能谱(XPS)等手段对复合物的物相、形貌、结构和表面化学态进行了表征。在1.00 mol·L^{-1} KOH+0.33 mol·L^{-1}尿素的电解液中，对复合物进行了电化学性能测试。同时，对构建的NiS(001)和Co,Cr-NiS(001)模型进行了密度泛函理论(DFT)计算，通过态密度(DOS)、d带中心以及UOR决速步(RDS)的能垒分析揭示了构效关系。电化学测试表明Co,Cr-NiS/CC复合物对UOR具有优异的催化活性，即在100 A·m^{-2}和1 000 A·m^{-2}的电流密度下，所需电位分别为1.321 V和1.378 V，低于其他对比样。在1.527 V的电位下，经过200 h的恒电位(CA)测试后，电流密度的保留率为64.83%。DFT计算表明，Co和Cr的共掺杂提高了复合物在费米能级(E_F)处DOS的强度，上移了复合物的d带中心，并将UOR的RDS的能垒降为0.331 eV，优化了NiS的电子结构及反应中间体的吸附能。本工作为构筑高效的非贵金属UOR催化剂提供了新思路。

关键词：Co，Cr-NiS/CC；共掺杂；尿素氧化反应；碱性电解质；密度泛函理论
中图分类号：O643.36　　**文献标识码：**A　　**doi:** 10.62756/jnuc.issn.1673-3193.2025.11.0028
引用格式：贾卓榕，张雨娟，胡拖平. 钴/铬共掺杂协同增强NiS的尿素电氧化性能[J]. 中北大学学报(自然科学版)，2026，47(3)：315-328.
JIA Zhuorong, ZHANG Yujuan, HU Tuoping. Co/Cr co-doping synergistically enhances the urea electrooxidation performance of NiS[J]. Journal of North University of China(Natural Science Edition), 2026, 47(3): 315-328.

Co/Cr Co-Doping Synergistically Enhances the Urea Electrooxidation Performance of NiS

JIA Zhuorong[1,2], ZHANG Yujuan[1,2], HU Tuoping[1,2*]

(1. School of Chemistry and Chemical Engineering, North University of China, Taiyuan, 030051, China;
2. Shanxi Provincial Key Laboratory of Hydrogen Energy Carbon-Based Electrode Materials, North University of China, Taiyuan 030051, China)

Abstract: During the process of hydrogen production from water-splitting assisted by the urea oxidation reaction (UOR), developing a high-performance nickel-based catalyst for UOR is a key challenge that must be addressed urgently to enhance hydrogen production efficiency. In this work, the Co/Cr co-doped

收稿日期：2025-11-26
基金项目：山西省重点实验室项目(202404010931028)；山西省科技合作与交流专项(202204041101028、202304041101025)；中央引导地方科技发展专项资金项目(YDZJSX2024D036)；山西省科技创新人才团队专项(202304051001003)
作者简介：贾卓榕(2000—)，女，硕士生，主要从事电化学催化的研究。
* **通信作者：**胡拖平(1969—)，男，教授，博士，主要从事纳米材料制备及其电催化的研究。E-mail：hutuoping@nuc.edu.cn。

nickel sulfide composite (Co, Cr-NiS/CC) was prepared on carbon cloth (CC) by the hydrothermal-calcination method. The composition, morphology, structure, and surface chemical state of the composite were characterized by X-ray diffraction (XRD), scanning electron microscopy (SEM), transmission electron microscopy (TEM), and X-ray photoelectron spectroscopy (XPS). The electrochemical performance of the composite was tested in the electrolyte of 1.00 mol·L^{-1} KOH and 0.33 mol·L^{-1} urea. Meanwhile, density functional theory (DFT) calculations were conducted on the NiS (001) and Co, Cr-NiS (001) models. The structure-activity relationship was revealed through the analysis of the density of states (DOS), the d-band center, and the energy barrier of the rate-determining step (RDS) for the UOR. Electrochemical tests demonstrate that the Co, Cr-NiS/CC composite exhibits excellent catalytic activity for UOR. Specifically, at the current densities of 100 A·m^{-2} and 1 000 A·m^{-2}, the required potentials are 1.321 V and 1.378 V, respectively, which are lower than those of the other control samples. At a potential of 1.527 V, after 200 h of chronoamperometry (CA) testing, the retention rate of current density is 64.83%. DFT calculations indicate that the co-doping of Co and Cr enhances the intensity of the DOS at the Fermi energy (E_F) of the composite, shifts the d-band center of the composite upwards, reduces the energy barrier of the RDS of UOR to 0.331 eV, and optimizes the electronic structure of NiS and the adsorption energy of reaction intermediates. This work proposes a new approach to constructing an efficient non-metallic UOR catalyst.

Key words: Co, Cr-NiS/CC; co-doping; urea oxidation reaction; alkaline electrolyte; density functional theory

0 Introduction

H_2 is a green and sustainable energy source[1-6] with high energy density and zero emissions[7-10]. Although hydrogen production through water electrolysis is environmentally friendly[11-13], it has some drawbacks such as the slow anode reaction kinetics[14-16] and the risk of hydrogen-oxygen mixture explosion. Highly efficient electrocatalysts have been developed to enhance the oxygen evolution reaction (OER) kinetics[17], there is still a gap from practical application[18]. For this reason, researchers have proposed using electrooxidation reactions with lower oxidation potentials to replace OER, including methanol, ethanol, hydrazine hydrate and urea[19-20]. The theoretical oxidation potential of the urea oxidation reaction (UOR) is only 0.370 V vs RHE[21-23], making it one of the most ideal alternative reactions to OER[24], as well as non-toxicity[25], low cost and high reserves of urea[26-27]. Therefore, the UOR-assisted water electrolysis for hydrogen production reduces the cost of electrolysis of water, and can treat urea-containing wastewater[28-30]. But, the complex 6-electron transfer process of UOR leads to its slow dynamics[31-32]. Many studies have shown that although precious metal (Pt, Ir, and Ru)-based catalysts exhibit excellent UOR activity[33], their scarce resources limit their wide application in business[34-36].

Nowadays, the focus of the study is to develop non-precious metal catalysts for the replacement of metal-based UOR catalysts. Ni-based composites (hydroxides, sulfides, oxides and phosphates)[37] exhibit excellent UOR activity[38-39]. For instance, the potential of UOR driven by the NiS-NiS_2 synthesized by Huang et al.[40] was only 1.280 V when the electrolyte was 1.00 mol·L^{-1} KOH+0.33 mol·L^{-1} urea and the current density (j) was 100 A·m^{-2}. Metal doping (such as Co, Fe, or Cu, etc.) can effectively enhance the UOR kinetics of Ni-based catalysts through synergistic effects such as electronic structure regulation, interface engineering and adsorption optimization. For example, the Sv-CoNiS@NF synthesized by Li et al.[41] in a mixed solution of 1.00 mol·L^{-1} KOH+0.33 mol·L^{-1} urea, only required a potential of 1.397 V to drive the j of 1 000 A·m^{-2}, which is because Co doping enhances the conductivity of the sample. Meanwhile, the presence of Co regulates the charge density at the interface of composite and enhances urea molecules'

adsorption capacity on the catalyst surface. The Fe-doped NiS-NiS_2 synthesized by Huang et al. [42] required a potential of 1.360 V in an alkaline medium and a j of 50 $A\cdot m^{-2}$, that is because Fe doping enhances the conductivity of the sample. In addition, Cr modulates the electron density distribution of Ni-based composites and promotes the UOR kinetics. For instance, the Cr-doped $NiSe_2$ composite ($Cr_{0.25}$-$NiSe_2$) synthesized by Zheng et al. [43] had a potential of only 1.370 V for UOR at a j of 1 000 $A\cdot m^{-2}$, that is because the Cr-induced the reconstruction of the surface to generate the highly active NiOOH phase. Metal doping significantly enhances the catalyst's UOR activity. However, the doping of a single metal still has relatively limited effects on improving the performance of catalysts, and there are relatively few studies on the co-doping of Co/Cr bimetals.

Based on the above background, in this study, Co/Cr co-doped NiS/CC composites (Co,Cr-NiS/CC) were successfully prepared by the hydrothermal-calcination method, and their performance was evaluated through structural characterization and electrochemical tests. To clarify the structure-activity relationship and the mechanism by which Co and Cr elements synergistically enhance the intrinsic activity of NiS through electronic structure regulation and adsorption energy optimization, the density of states (DOS) and the free energy changes (ΔG) at each step of UOR were calculated and analyzed through theoretical calculations.

1 Experiment

1.1 Chemicals and reagents

Chromium nitrate [$Cr(NO_3)_2\cdot 9H_2O$], potassium hydroxide (KOH), cobalt nitrate [$Co(NO_3)_2\cdot 6H_2O$], nickel nitrate [$Ni(NO_3)_2\cdot 6H_2O$], thiourea (CH_4N_2S) and urea [$CO(NH_2)_2$] were all obtained from Tianjin damao chemical reagent company, with purity of analytical grade. All reagents were used directly without purification.

1.2 Optimization of experimental conditions

To prepare cost-effective catalytic materials with superior performance, various metals underwent performance testing. LSV measurements were conducted on Co, Cr-NiS/CC samples and individual metals in both 1.00 $mol\cdot L^{-1}$ KOH and 1.00 $mol\cdot L^{-1}$ KOH+0.33 $mol\cdot L^{-1}$ urea electrolyte solutions. The Cr-NiS/CC exhibits superior UOR catalytic activity compared to the Co, Cr, and Ni monometals. Consequently, the metal selection for the sample was determined to be a combination of Co, Cr, and Ni.

After selecting suitable metals, performance tests were conducted on different combinations of Co, Cr, and Ni to prepare cost-effective catalytic materials with superior properties. LSV tests were performed on these metal combinations in both 1.00 $mol\cdot L^{-1}$ KOH and 1.00 $mol\cdot L^{-1}$ KOH+0.33 $mol\cdot L^{-1}$ urea electrolyte solutions. The molar ratio of Co∶Cr∶Ni at 1∶1∶6 exhibited the highest UOR catalytic activity compared to other metal combinations. Therefore, $n_{Co}:n_{Cr}:n_{Ni}=1:1:6$ was selected for the final sample composition.

To investigate the effects of different calcination temperatures and durations on the catalytic performance of Co, Cr-NiS/CC samples, LSV tests were conducted on these samples calcined at varying temperatures and times in 1.00 $mol\cdot L^{-1}$ KOH and 1.00 $mol\cdot L^{-1}$ KOH+0.33 $mol\cdot L^{-1}$ urea electrolyte solutions. The Co, Cr-NiS/CC sample exhibited the best UOR catalytic activity at a calcination temperature of 400 ℃ and a calcination time of 2 h. Therefore, the calcination temperature was selected as 400 ℃ and the calcination time as 2 h.

To investigate the effects of different hydrothermal temperatures and durations on the catalytic performance of Co, Cr-NiS/CC samples, LSV tests were conducted on these samples under various hydrothermal conditions in 1.00 $mol\cdot L^{-1}$ KOH and 1.00 $mol\cdot L^{-1}$ KOH+0.33 $mol\cdot L^{-1}$ urea electrolyte solutions. The Co, Cr-NiS/CC sample exhibited the best UOR catalytic activity at a hydrothermal temperature of 180 ℃ and a hydrothermal time of 5 h. Therefore, the hydrothermal temperature was selected as 180 ℃ and the hydrothermal time as 5 h.

1.3 Synthesis of Co, Cr-NiS/CC samples

Carbon cloth (CC) (1 cm×2 cm) was pretreated by the literature method[44]. Dissolve $Co(NO_3)_2·6H_2O$ (0.5 mmol), $Cr(NO_3)_2·9H_2O$ (0.5 mmol), $Ni(NO_3)_2·6H_2O$ (3 mmol), CH_4N_2S (1.5 mmol) and $CO(NH_2)_2$ (1.5 mmol) in 15 mL of deionized water. Subsequently, the obtained solution was transferred together with CC to a 25 mL autoclave for hydrothermal reaction at 180 ℃ for 5 h. After the hydrothermal reaction was completed, the CC was alternately rinsed with water and ethanol three times, and then dried at 60 ℃ to obtain CC containing the precursor, which was put in a porcelain boat and pyrolyzed at a certain temperature for 2 h under N_2 atmosphere to prepare Co, Cr-NiS/CC samples (Fig. 1).

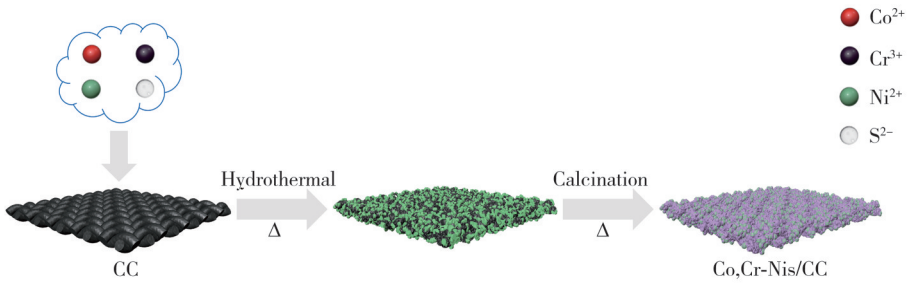

Fig. 1 Synthesis schematic of Co, Cr-NiS/CC

The synthesis process of the control samples was the same as that of the Co, Cr-NiS/CC. The only difference lies in that during the synthesis process: thiourea was not added to Co, Cr-NiO/CC; $Ni(NO_3)_2·6H_2O$ was not added to Co, Cr/CC; $Cr(NO_3)_2·9H_2O$ was not added to Co-NiS/CC; $Co(NO_3)_2·6H_2O$ was not added to Cr-NiS/CC; $Co(NO_3)_2·6H_2O$ and $Cr(NO_3)_2·9H_2O$ were not added to NiS/CC.

1.4 Structural characterization

In this work, the instruments and their models, and the methods used to characterize the crystal phase, composition, morphology, surface elements, and valence states of the composites were similar to those in the literature.

1.5 Characterization of electrochemical performance

Except for the different potential range (0.627~0.677 V) during the cyclic voltammetry (CV) test for fitting the double-layer capacitance (C_{dl}), other test methods of the electrochemical performance test were consistent with those in previous literature[44].

1.6 Density functional theory calculation

DFT calculations were carried out to adopt the DMol^3 module in the Materials Studio software. A 5×5 NiS (001) supercell model was constructed, and the Co and Cr-NiS models were built by replacing atoms. The methods and parameters of other DFT calculations were consistent with those in previous literature[45].

2 Results and discussion

2.1 Structural characterization

As exhibited in Fig. 2, the X-ray diffraction (XRD) patterns of Co, Cr-NiS/CC, Co-NiS/CC and Cr-NiS/CC samples are well matched with the NiS standard cards (PDF#12-0041 and 02-1280), confirming the successful preparation of NiS.

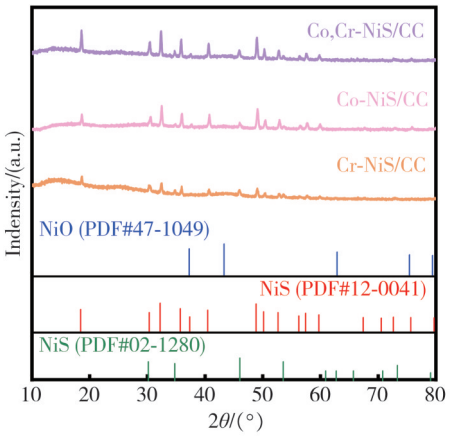

Fig. 2 XRD pattern

As shown in Fig. 3（a）, scanning electron microscope（SEM）images show that Co,Cr-NiS/CC present the morphology of nanoparticles anchored on CC. The high-resolution transmission electron microscope（HRTEM）characterization shown in Fig. 3(b), the lattice spacing of 0.171 nm corresponds to the NiS（110）crystal plane, and the selected area electron diffraction（SAED）pattern in Fig. 3（c）further confirms the polycrystalline properties of NiS. As shown in Fig. 3(d), the energy dispersion spectrum（EDS）element mapping indicates that C, O, S, Cr, Ni and Co elements are uniformly distributed in Co,Cr-NiS/CC.

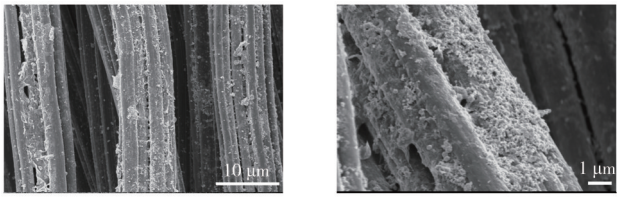

（a）SEM image

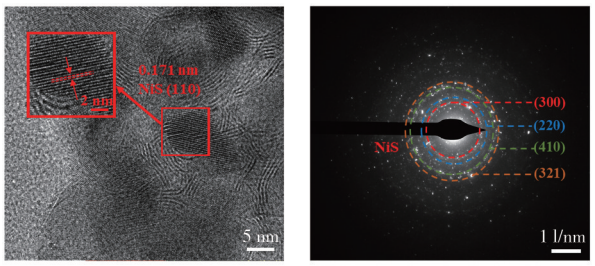

（b）TEM image　（c）SAED image

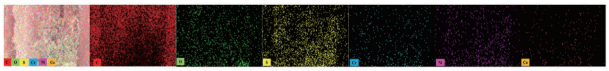

（d）SEM-EDS mapping images of C, O, S, Cr, Ni and Co in Co,Cr-NiS/CC

Fig. 3　Morphological characterization of Co,Cr-NiS/CC

The full X-ray photoelectron spectroscopy（XPS）spectrum of Co,Cr-NiS/CC samples（Fig. 4）consist of Ni 2p, Co 2p, Cr 2p, O 1s, C 1s, and S 2p spectra. As shown in Fig. 5(a), two peaks of Co $2p_{3/2}$（Co^{2+}/Co^{3+}）are located at 781.01 eV and 774.00 eV, respectively. The peaks at 797.67 eV and 795.15 eV correspond to Co $2p_{1/2}$（Co^{2+}/Co^{3+}）, and the peaks at 786.00 eV and 802.23 eV are satellite peaks of Co. Compared with the Co,Cr-NiO/CC and Co-NiS/CC samples, the two peaks of Co in the Co, Cr-NiS/CC sample shift by 0.69 eV and 0.22 eV respectively towards the low bonding energy direction. Moreover, the ratio of Co^{3+}/Co^{2+} peak areas（0.31）is greater than that of Co,Cr-NiO/CC（0.25）and Co-NiS/CC（0.21）, indicating that the composite contains more Co^{3+} [46-48].

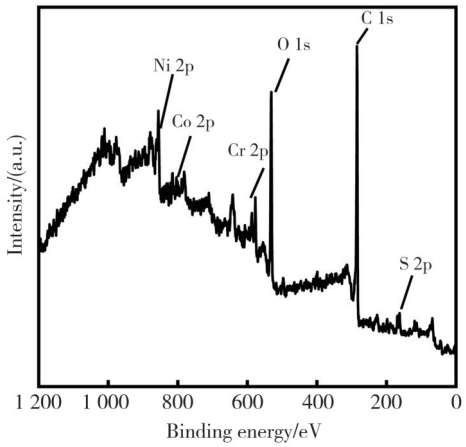

Fig. 4　Full XPS spectrum of Co,Cr-NiS/CC

In Fig. 5(b), peaks at 576.68 eV and 578.13 eV correspond to Cr $2p_{3/2}$（Cr^{3+}/Cr^{6+}）, while those at 586.45 eV and 588.29 eV correspond to Cr $2p_{1/2}$（Cr^{3+}/Cr^{6+}）. Compare with the Co,Cr-NiO/CC and Cr-NiS/CC samples, the two peaks of Cr in the Co, Cr-NiS/CC sample shift by 0.26 eV and 0.22 eV respectively towards the high bonding energy direction. Moreover, the ratio of Cr^{6+}/Cr^{3+} peak areas（0.96）is greater than that of Co,Cr-NiO/CC（0.27）and Cr-NiS/CC（0.62）, indicating that the composite contains more Cr^{6+} [48].

Fig. 5(c) reveals that two peaks of Ni $2p_{3/2}$（Ni^0/Ni^{2+}）are located at 853.25 eV and 855.95 eV, respectively. Meanwhile, the peaks at 870.25 eV and 873.73 eV correspond respectively to Ni $2p_{1/2}$（Ni^0/Ni^{2+}）. Two satellite peaks of Ni $2p_{3/2}$ and Ni $2p_{1/2}$ are located at 861.68 eV and 879.99 eV, respectively. Compare with the Co-NiS/CC samples, the Ni peak in the Co,Cr-NiS/CC samples shift 0.15 eV towards the high bonding energy direction, while compare with the Cr-NiS/CC samples, the Ni peak in the Co,Cr-NiS/CC samples shift by 0.07 eV towards the low bonding energy direction. Furthermore, the ratio of the Ni^{2+}/Ni^0 peak areas in the Co, Cr-NiS/CC samples（9.09）is greater than that in Co-NiS/CC（4.35）and Cr-NiS/CC（5.4）, indicating that the composite contains more Ni^{2+}, which is one of the

reasons for its higher activity[49-51].

In Fig. 5(d) of the C 1s spectrum, the C—C, C—O—C and O—C=O peaks are located at 284.85, 285.40, and 286.08 eV, respectively[52]. Fig. 5(e) of the S 2p spectrum shows S^{2-} $2p_{3/2}$, S^{2-} $2p_{1/2}$, S—O $2p_{3/2}$, and S—O $2p_{1/2}$ peaks at 161.75, 163.25, 168.25, and 169.23 eV, respectively, which indicates the Co,Cr-NiS/CC sample contains the S element[53]. As shown in Fig. 5(f), in the O 1s spectrum, peaks locate at 531.27, 532.51, and 533.65 eV belong to oxygen of metal-O bonds, metal—OH bonds and H_2O, respectively[53-54].

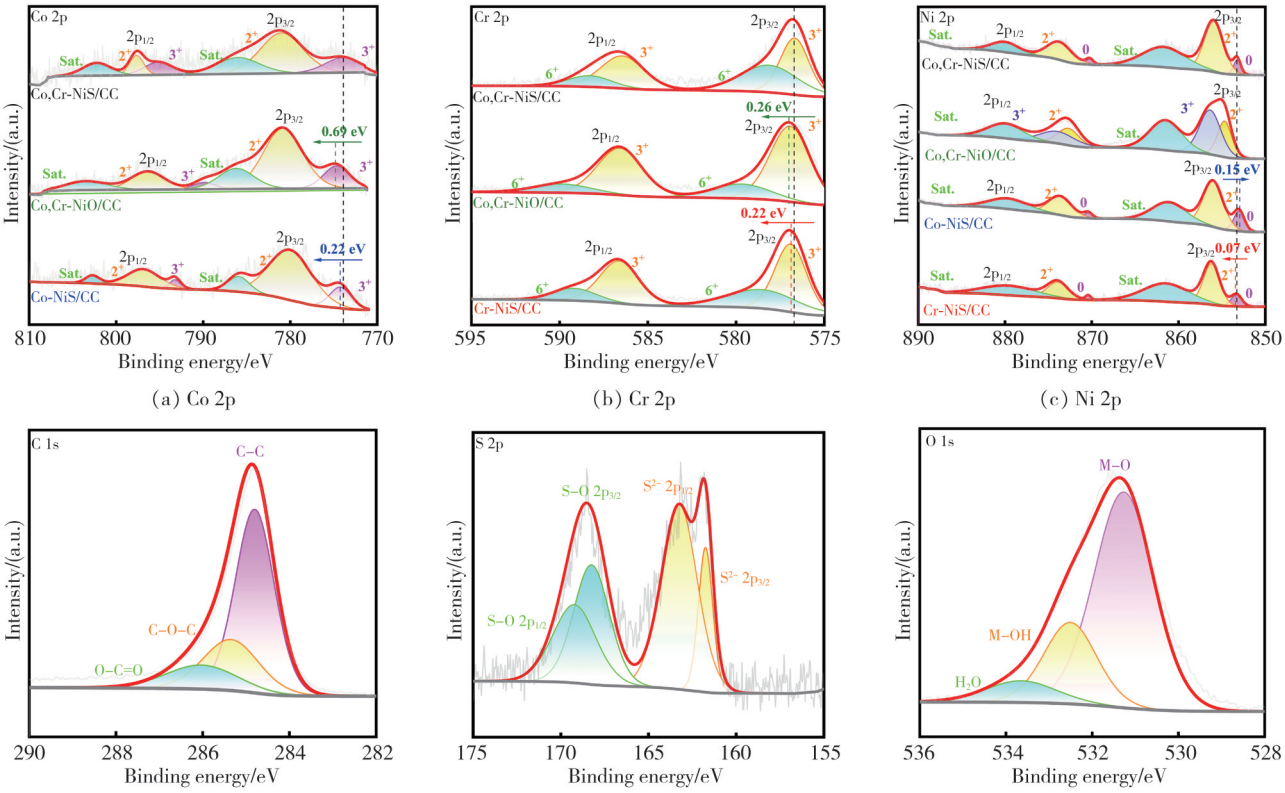

Fig. 5 XPS spectrum of Co,Cr-NiS/CC

2.2 Electrochemical UOR performance testing

LSV curves of Co,Cr-NiS/CC are shown in Fig. 6(a), it can be seen that in the electrolyte of 1.00 mol·L^{-1} KOH, when the j is 100 or 1 000 A·m^{-2}, the potentials required by OER are 1.522 or 1.621 V, respectively. When 0.33 mol·L^{-1} urea was added, the corresponding potentials significantly decreased to 1.321 V and 1.378 V. It indicates that from a thermodynamic perspective, UOR occurs superior to OER. As shown in Fig. 6(b) and Fig. 6(c), all LSV tests were conducted based on three parallel experiments to ensure data reproducibility. As shown in Fig. 6(c), the error bars shown in the figure represent the standard deviation of the three experimental results. At the same j (100 or 1 000 A·m^{-2}), the UOR initial potentials of Co,Cr-NiS/CC ((1.321±0.006)/(1.378±0.003) V) are significantly lower than those of Co-NiS/CC ((1.392±0.003)/(1.463±0.001) V), Cr-NiS/CC ((1.404±0.003)/(1.479±0.002) V), Co,Cr-NiO/CC ((1.414±0.003)/(1.512±0.001) V), NiS/CC ((1.580±0.006)/(1.686±0.007) V) and Co,Cr/CC ((1.873±0.014)/(2.364±0.003 V)), confirming that Co,Cr-NiS/CC had the optimal UOR catalytic activity. Furthermore, the data used in Fig. 6(c) is the average of three results under the same conditions. As shown in Fig. 7, at a potential of 1.467 V, the current density (j_{OER}, 25.9 A·m^{-2}) of OER in the electrolyte of 1.00 mol·L^{-1} KOH and the total current density (j_{total}, 423.9 A·m^{-2}) after adding 0.33 mol·L^{-1} urea to the KOH electrolyte were

measured respectively. In this way, the selectivity of UOR = $(j_{total}-j_{OER})/j_{total}$ = 93.89%.

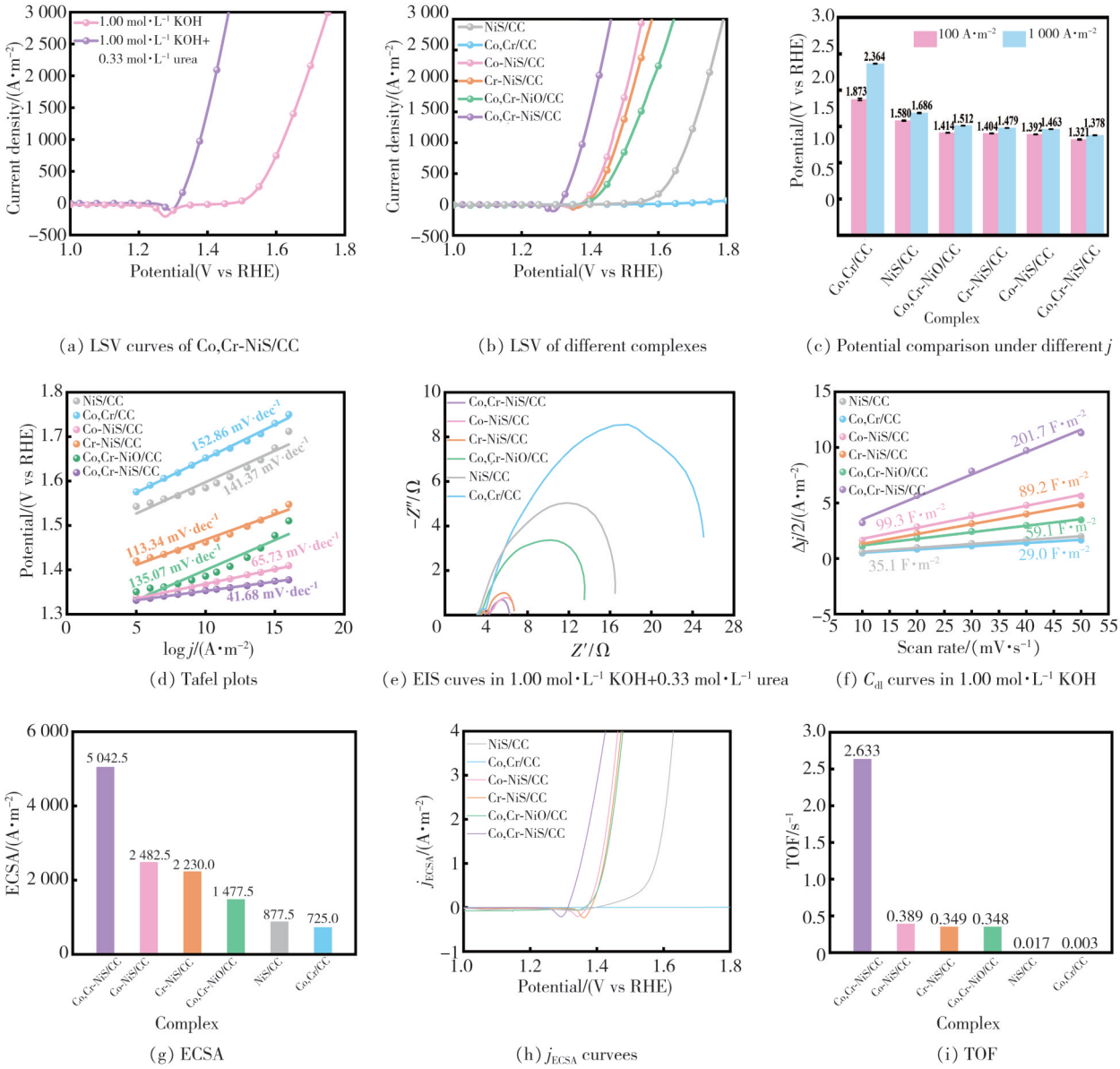

(a) LSV curves of Co,Cr-NiS/CC　(b) LSV of different complexes　(c) Potential comparison under different *j*

(d) Tafel plots　(e) EIS cuves in 1.00 mol·L⁻¹ KOH+0.33 mol·L⁻¹ urea　(f) C_{dl} curves in 1.00 mol·L⁻¹ KOH

(g) ECSA　(h) j_{ECSA} curvees　(i) TOF

Fig. 6　Electrochemical test plots for different complexes

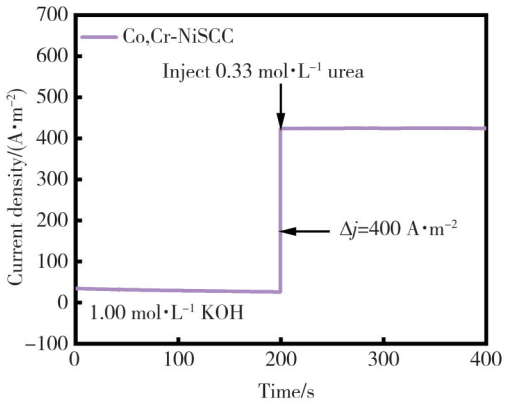

Fig. 7　CA test of Co,Cr-NiS/CC

As shown in Fig. 6(d) and Fig. 8, the chronopotentiometry (CP) curve was fitted to compare the Tafel slope[54]. The Tafel slope of Co,Cr-NiS/CC (41.68 mV·dec^{-1}) is significantly inferior to that of Co-NiS/CC (65.73 mV·dec^{-1}), Cr-NiS/CC (113.34 mV·dec^{-1}), Co, Cr-NiO/CC (135.07 mV·dec^{-1}), NiS/CC (141.37 mV·dec^{-1}) and Co,Cr/CC (152.86 mV·dec^{-1}), showing that its UOR kinetic process is the fastest[55-56]. As shown in Fig. 6(e), the charge transfer resistance (R_{ct}) of Co,Cr-NiS/CC (1.96 Ω) is much smaller than that of the control samples Co-NiS/CC (2.28 Ω), Cr-NiS/CC (2.64 Ω), Co,Cr-NiO/CC (10.18 Ω), NiS/CC (13.44 Ω) and Co,

Cr/CC (21.26 Ω), confirming that it has the optimal electronic transport capacity. This is attributed to the fact that the Co and Cr optimize the electron density of NiS and enhances its conductivity, which is highly consistent with the XPS and total DOS characterization results[57].

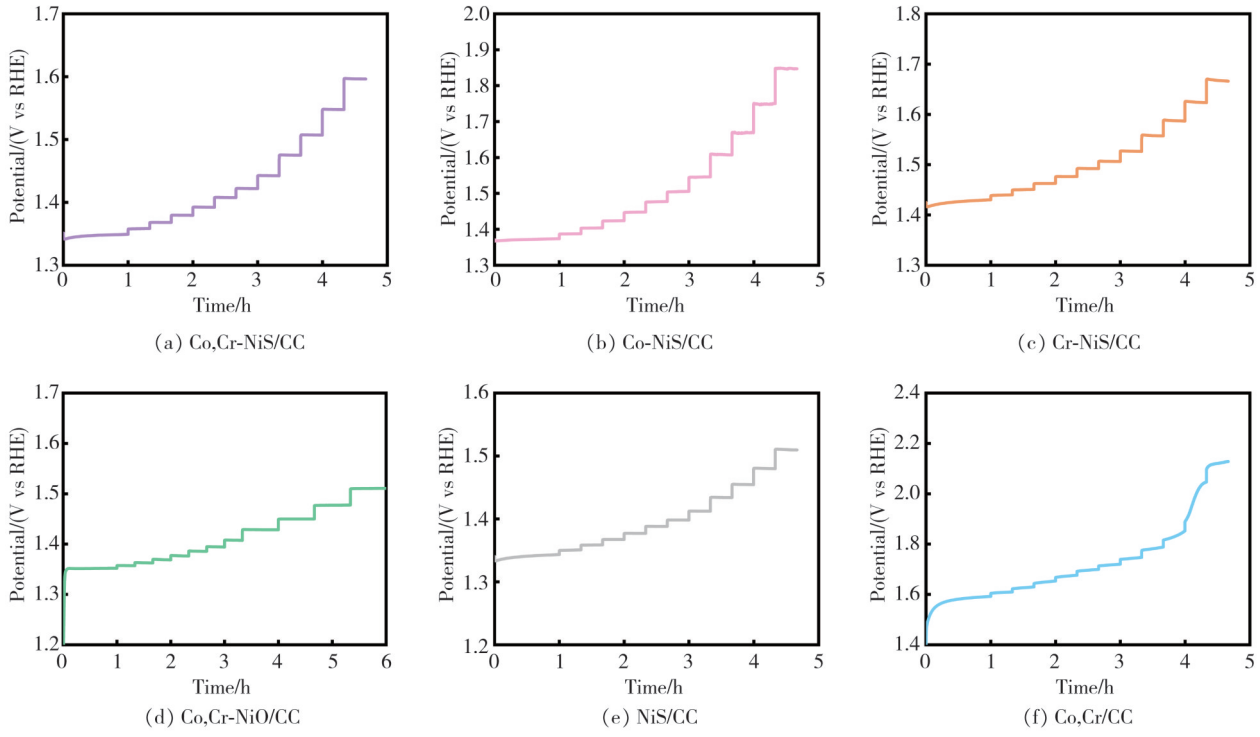

Fig. 8 CP curves of different complexes

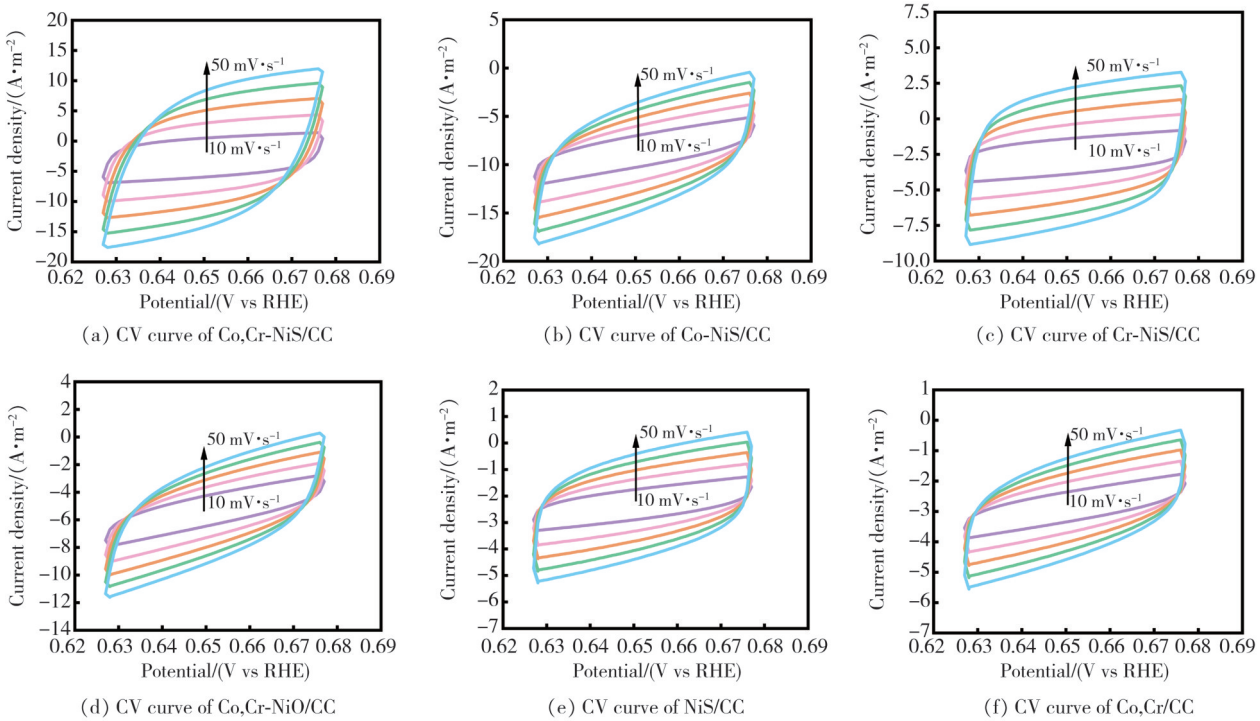

Fig. 9 Electrochemical double-layer capacitance test diagram

As shown in Fig. 6(f) and Figs. 9(a)~9(f), the C_{dl} value[58] of Co, Cr-NiS/CC (201.7 F·m^{-2}) is significantly greater than that of Co-NiS/CC (99.3 F·m^{-2}), Cr-NiS/CC (89.2 F·m^{-2}), Co,Cr-NiO/CC (59.1 F·m^{-2}), NiS/CC (35.1 F·m^{-2}) and Co,Cr/CC (29.0 F·m^{-2}). Since C_{dl} is proportional to the electrochemical active surface area (ECSA), as can be seen from Fig. 6(g), the ECSA value of Co,Cr-

NiS/CC（5 042.5 A·m^{-2}）is also the largest. This indicates that Co, Cr-NiS/CC has exposed more reaction sites for the UOR. From Fig. 6(h) and Fig. 6(i), it can be seen that the j_{ECSA} results obtained by further normalizing the j through ECSA showed that the j_{ECSA} and the TOF value of Co,Cr-NiS/CC are the highest. These results indicate that the activity of Co,Cr-NiS/CC composite is the highest. This is owing to the Co and Cr can regulat the electronic distribution of NiS and significantly enhance its intrinsic catalytic performance. Fig. 10(a) shows that after 1 500 CV cycles, the potentials of the Co,Cr-NiS/CC samples increase by 0.08%（100 A·m^{-2}）and 0.44%（1 000 A·m^{-2}）, respectively. As shown in Fig. 10(b), after 200 h of CA test, the activity retention rate of Co, Cr-NiS/CC is 64.83%, indicating its excellent stability.

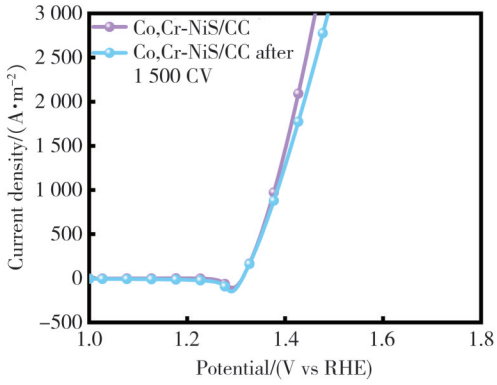

(a) LSV curves

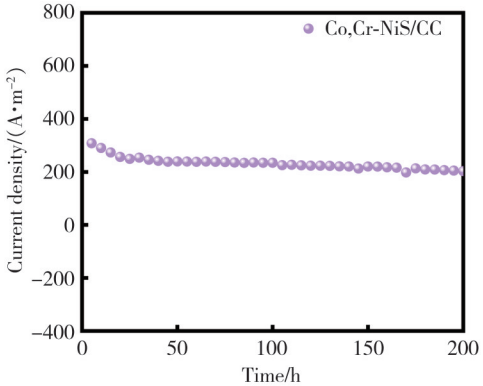

(b) CA test in 1.00 mol·L^{-1} KOH+0.33 mol·L^{-1} urea

Fig. 10　Stability testing of Co,Cr-NiS/CC

2.3　Post-CA structural characterization

The XRD in Fig. 11 and the HRTEM of the samples after CA testing in Fig. 12(a) confirmed that the NiS phase is basically retained, and lattice fringes of the NiS (300) crystal plane are also present, indicating that the main structure of the samples is stable. In Fig. 12(b) and Fig. 12(c), SEM shows the surface roughness and agglomeration of Co, Cr-NiS/CC samples, which is attributed to the corrosive effect of KOH. In Figs. 13(a)～13(d), XPS revealed that peaks of Co 2p and Cr 2p shift by 0.71 eV and 1.03 eV respectively towards the high bonding energy direction. The Ni^0 peak disappeared and the Ni^{3+} peak was generated. The S^{2-} peak is weakened along with the enhancement of the S—O peak, indicating that partial oxidation and dissolution of Cr and S are the main reasons for the decline in activity.

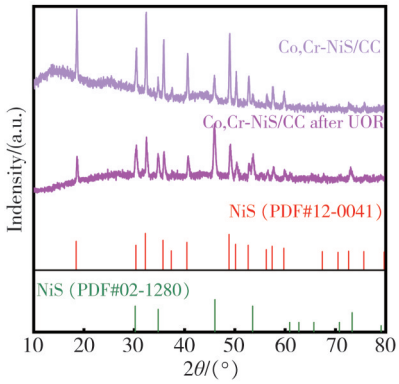

Fig. 11　XRD curves of Co,Cr-NiS before and after CA treatment

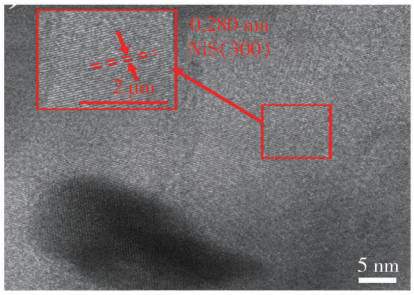

(a) TEM image of Co,Cr-NiS/CC after CA

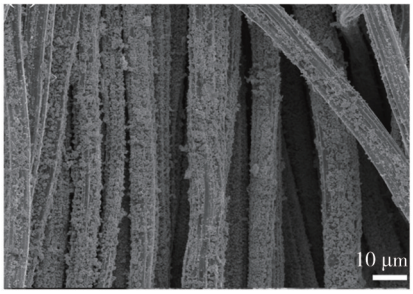

(b) SEM image of Co,Cr-NiS/CC after CA

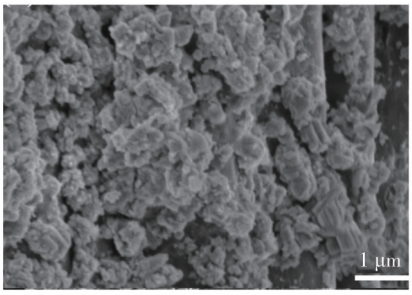

(c) Enlarged view of SEM

Fig. 12 Morphological characterization of different samples

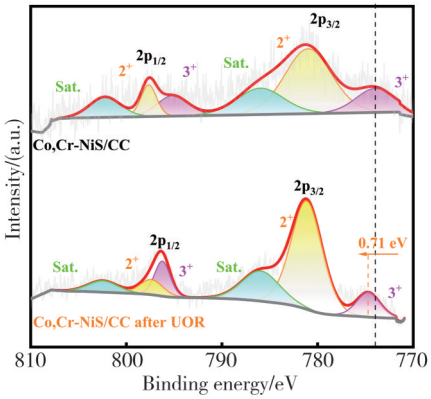

(a) Co 2p

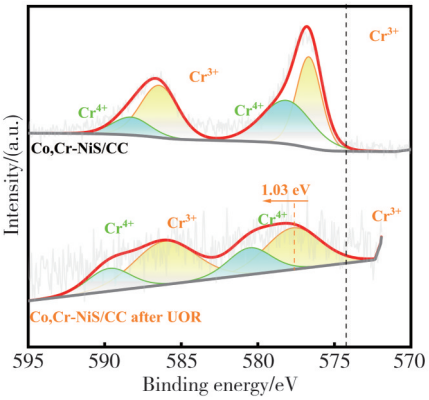

(b) Cr 2p

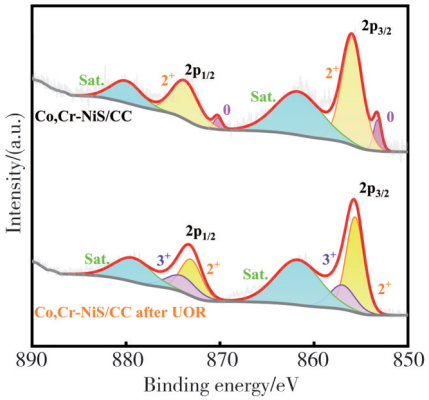

(c) Ni 2p

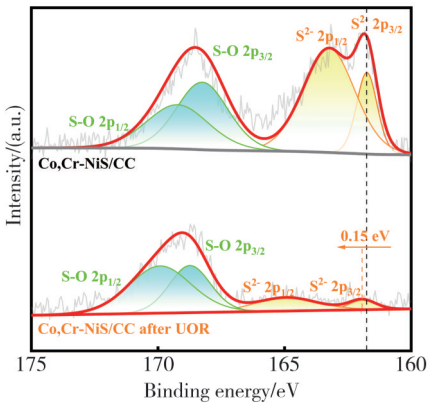

(d) S 2p

Fig. 13 XPS spectrum of Co,Cr-NiS/CC after CA

2.4 DFT calculations

To further reveal the structure-activity relationship of Co,Cr-NiS catalysts, as shown in Fig. 14 and Fig. 15, NiS (001) and Co,Cr-NiS (001) models were constructed, and their structures were optimized by theoretical calculations.

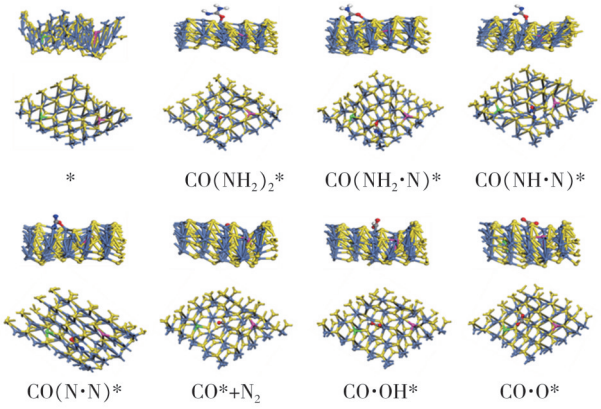

Fig. 14 Adsorption models of Co,Cr-NiS on adsorbents

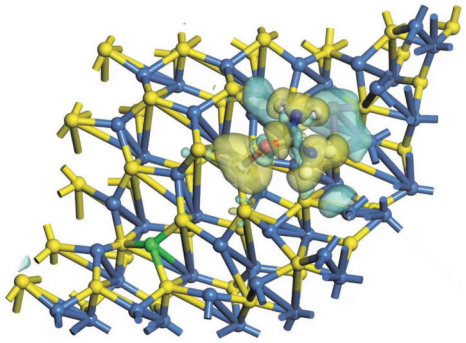

Fig. 15 Differential charge density analysis of Co,Cr-NiS

As can be seen from Fig. 16(a) and Tab. 1, for the Co,Cr-NiS (001) samples, the energy barrier (0.331 eV) of the rate-determining step (RDS) is significantly lower than that of NiS (001)

（0.423 eV），which is consistent with the activity[59]. Fig. 16(b) shows that the total DOS of Co, Cr-NiS (001) at the Fermi level (EF) has a higher intensity (62.607) than that of NiS (001) (61.800), indicating that it has better electrical conductivity. This can be confirmed by electrochemical impedance spectroscopy (EIS) in Fig. 6(e). As shown in Fig. 16(c), the d-band center of Co, Cr-NiS (001) (−1.175 eV) is closer to EF than that of NiS (001) (−1.224 eV)[60], indicating that Co and Cr modulate the electronic distribution of NiS (001) and optimize the adsorption and desorption processes of the intermediate.

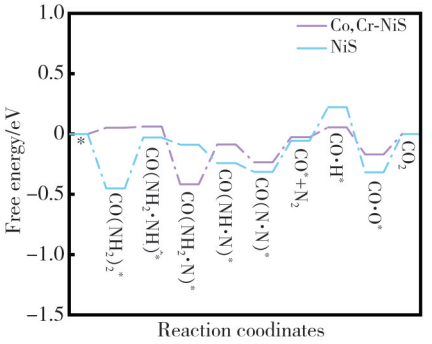

(a) UOR steps

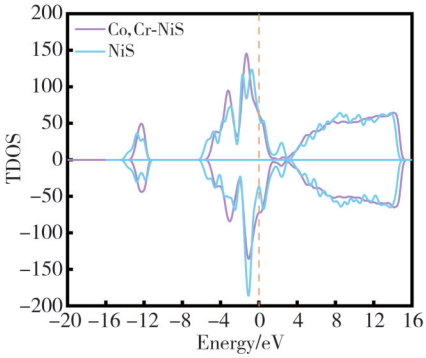

(b) DOS

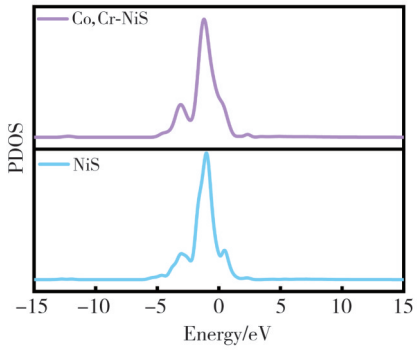

(c) d-bands

Fig. 16　DFT calculation diagrams of NiS and Co/Cr-doped NiS

Tab. 1　Gibbs free energy change (ΔG) of the UOR elementary steps on the Co,Cr-NiS and NiS

Elementary step	ΔG/eV	
	Co,Cr-NiS	NiS
*	0.000	0.000
$^*+CO(NH_2)_2 \rightarrow CO(NH_2)_2^*$	0.052	−0.452
$CO(NH_2)_2^* \rightarrow CO(NH_2{\cdot}NH)^*+H$	0.062	−0.029
$CO(NH_2{\cdot}NH)^* \rightarrow CO(NH_2{\cdot}N)^*+H$	−0.417	−0.088
$CO(NH_2{\cdot}N)^* \rightarrow CO(NH{\cdot}N)^*+H$	−0.086	−0.241
$CO(NH{\cdot}N)^* \rightarrow CO(N{\cdot}N)^*+H$	−0.234	−0.314
$CO(N{\cdot}N)^* \rightarrow CO^*+N_2$	−0.026	−0.055
$CO^*+OH \rightarrow CO{\cdot}OH^*$	0.056	0.223
$CO{\cdot}OH^* \rightarrow CO{\cdot}O^*+H$	−0.169	−0.317
$CO{\cdot}O^* \rightarrow CO{\cdot}O+*$	0.000	0.000

In summary, Co/Cr co-doping regulates the electronic structure of NiS, reduces the UOR RDS energy barrier, and enhances the intrinsic activity of NiS.

Tab. 2　Comparison of the catalytic performance between Co,Cr-NiS/CC and catalysts reported in selected literature

Catalyst	Potential/V	Current density/(A·m^{-2})	Current density retention/%	Duration/h
S_v-CoNiS@NF[41]	1.397	1 000	—	
Fe-doped NiS-NiS_2[42]	1.360	500	—	
NiCoCr-LDH/NF[61]	1.380	1 000	95.30	50
Ni/NiO/NiB@NC-500[62]	1.370	100	84.58	12
NiO-CrO@N-C[63]	1.370	100	83.00	8
Cr-NiO/CWF[64]	1.360	100	90.00	12
Co,Cr-NiS/CC (this work)	1.321	100	94.31	8
	1.351	500	90.45	12
	1.378	1 000	64.23	50
			64.83	200

3　Conclusion

In this work, Co/Cr co-doped NiS/CC composites (Co, Cr-NiS/CC) were prepared through doping strategies. The electrochemical performance indicated that the activity and durability of the composite are comparable to or higher than those previously reported in the references. This is mainly due to the combined effect of Co and Cr. Furthermore, DFT calculations further revealed that co-doping of Co/Cr tuned the electron density distribution of NiS and reduced the energy barrier of RDS. This study provides new ideas and preparation methods for designing highly efficient and stable NiS-based UOR electrocatalysts.

利益冲突声明/Conflict of Interests

所有作者声明不存在利益冲突。

All authors declare no relevant conflict of interests.

References:

[1] WEI L, ZHANG L, LI L, et al. Tuning built-in potential of NiP/NiFe LDH p-n junction towards efficient electrocatalytic water and urea oxidation[J]. International Journal of Hydrogen Energy, 2024, 82: 64-72.

[2] ZHANG T, LIU S, CAI W, et al. Utilizing cationic vacancies to enhance nickel-cobalt layered double hydroxides for efficient electrocatalytic urea oxidation reaction[J]. Chemical Engineering Journal, 2024, 500: 156766.

[3] WEN W, DU X, ZHANG X. Preparation of Zr doped NiFe LDH@$NiFe_2O_4$/NF as environmentally friendly and robust water and urea oxidation reaction electrocatalyst [J]. International Journal of Hydrogen Energy, 2024, 81: 615-623.

[4] ZHANG Y, ZHANG Y, ZHANG X, et al. pH-induced two Co(II) metal - organic frameworks with different topologies: magnetism and CO_2/CH_4 separation [J]. Crystal Growth & Design, 2024, 24(16): 6673-6681.

[5] ZHANG J, BUSARI F K, ZHANG Y, et al. RuO_x clusters anchored on self-assembled SnO_2 cubic nanocage for boosting sustainable acidic water oxidation[J]. Nano Research Energy, 2025, 4(1): e9120140.

[6] GU Y, ZHANG Y, SONG X, et al. Fluorine-induced surface protection strategy for bifunctional high entropy electrocatalysts enables stable seawater splitting[J]. Nano Research Energy, 2025, 4(4): e9120189.

[7] ZHONG M, YANG J, XU M, et al. Significantly enhanced energy-saving H_2 production coupled with urea oxidation by low- and non-Pt anchored on NiS-based conductive nanofibers[J]. Small, 2024, 20(1): 2304782.

[8] LI Y, WANG X, LI C, et al. Al-etching-induced defect engineering in NiAl LDHs for promoting multifunctional electrocatalytic oxidations: Water oxidation and urea oxidation[J]. International Journal of Hydrogen Energy, 2024, 90: 1041-1050.

[9] FATHOLLAHI A, SHAHRABI T, DARBAND G B. Modulation of active surface sites on Ni - Fe - S by the dynamic hydrogen bubble template method for energy-saving hydrogen production [J]. Journal of Materials Chemistry A, 2024, 12(15): 9038-9054.

[10] ZHOU X, YANG T, LI T, et al. *In—situ* fabrication of carbon compound NiFeMo-P anchored on nickel foam as bi-functional catalyst for boosting overall water splitting [J]. Nano Research Energy, 2023, 2: e9120086.

[11] LI B, YANG Y, ZHANG M, et al. Novel nickel-doped $CoMn_xSe_2$ Chalcogenides for boosting hydrogen evolution and urea oxidation[J]. International Journal of Hydrogen Energy, 2024, 51: 1208-1215.

[12] JING X, MU Y, GAO Z, et al. Intermetallic ferric nickel silicide alloy derived from magadiite by magnesiothermic reaction as bifunctional electrocatalyst for overall water splitting [J]. Nano Research Energy, 2024, 3(2): e9120104.

[13] YANG S, LUO J, XU Y, et al. Oxygen evolution reaction performance misjudgment caused by the self-oxidation process[J]. Nano Research Energy, 2024, 3(4): e9120136.

[14] SHI X, ZHOU D, CHEN G, et al. Novel gel method MXene-supported dual-site PtNi-NiO for electrocatalytic water reduction and urea oxidation[J]. Small, 2025, 21(1): 2409461.

[15] ZHANG H, DING H, WANG W, et al. Air plasma activation of catalytic sites within MXene nanosheets for oxygen evolution and urea oxidation catalysis [J]. Materials Today Energy, 2024, 44: 101623.

[16] GAO X, WANG P, SUN X, et al. Membrane-free water electrolysis for hydrogen generation with low cost [J]. Angewandte Chemie International Edition, 2025, 64(6): e202417987.

[17] JIA R, TAN Y, LI A, et al. 3D ordered RuO_2/WO_3 heterostructure inverse opal arrays for highly-active and stable acidic oxygen evolution reaction [J]. Nano Research Energy, 2025, 4(1): e9120141.

[18] XU S, JIAO D, RUAN X, et al. Synergistic modulation of the d-band center in Ni_3S_2 by selenium and iron for enhanced oxygen evolution reaction (OER) and urea oxidation reaction (UOR)[J]. Journal of Colloid and Interface Science, 2024, 671: 46-55.

[19] MAHESKUMAR V, MIN A, MOON C J, et al. Modulating the electronic structure of Ni/NiO nano-composite with high-valence Mo doping for energy-saving hydrogen production *via* boosting urea oxidation kinetics [J]. Small Structures, 2023, 4(12): 2300212.

[20] SHI J, WEI T, YAN X, et al. Constructing efficient-active-centers selenide heterointerface for enhanced urea oxidation-driven hydrogen evolution [J]. International Journal of Hydrogen Energy, 2025, 127: 576-585.

[21] CHEN L, WANG L, REN J T, et al. Artificial heterointerfaces with regulated charge distribution of Ni active sites for urea oxidation reaction[J]. Small Meth-

ods, 2024, 8(12): 2400108.

[22] WANG P, ZHENG W, QU Y, et al. Photo-excited high-spin state Ni(III) species in Mo-doped Ni_3S_2 for efficient urea oxidation reaction[J]. Small, 2024, 20(45): 2403107.

[23] ZHANG Z, TAN D, WANG J, et al. Co_2P-NiMoN/NF heterostructure nanorod arrays as efficient bifunctional electrocatalysts for urea electrolysis[J]. ACS Applied Materials & Interfaces, 2025, 17(10): 15480-15491.

[24] LIU H, WANG P, QI X, et al. Accumulated charge density at the interface boosts the urea oxidation reaction activity of Ni_3N/Ni_3S_2 heterointerface [J]. Chemical Engineering Journal, 2024, 491: 152160.

[25] LIU Q, ZHAO F, YANG X, et al. Constructing interlaced network structure by grain boundary corrosion methods on CrCoNiFe alloy for high-performance oxygen evolution reaction and urea oxidation reaction[J]. Journal of Materials Science & Technology, 2024, 203: 97-107.

[26] LI X, LIN H, HUANG W, et al. Enhanced urea oxidation catalysis through Ni single-atom doping on Cu_2O surfaces: A computational study[J]. Journal of Materials Chemistry A, 2024, 12(26): 15874-15884.

[27] WU T H, QIU Z T, HSIEH C N, et al. An organic - inorganic heterojunction electrocatalyst for highly efficient urea oxidation[J]. Journal of Materials Chemistry A, 2024, 12(37): 25186-25192.

[28] KIM M, MIN K, KO D, et al. Regulating the electronic structure of Ni_2P by one-step Co, N dual-doping for boosting electrocatalytic performance toward oxygen evolution reaction and urea oxidation reaction[J]. Journal of Colloid and Interface Science, 2023, 650: 1851-1861.

[29] ZHAO Z, DONG Y, DING H, et al. Manganese-facilitated dynamic active-site generation on Ni_2P with self-termination of surface reconstruction for urea oxidation at high current density[J]. Water Research, 2024, 253: 121266.

[30] LI X, FENG G, CHEN Y, et al. Hybrid hydrovoltaic electricity generation driven by water evaporation[J]. Nano Research Energy, 2024, 3(2): e9120110.

[31] DUAN N, HOU T, ZHENG W, et al. Insight into the structure of Mn-NiS_2 during urea oxidation using combined *in situ* X-ray absorption spectroscopy and attenuated total reflectance surface-enhanced infrared absorption spectroscopy[J]. ACS Catalysis, 2024, 14(3): 1384-1393.

[32] HU Y, SHAO L, JIANG Z, et al. Unveiling the role of boron on nickel-based catalyst for efficient urea oxidation assisted hydrogen production[J]. Advanced Functional Materials, 2024, 34(52): 2411011.

[33] KALAIYARASAN G, LEE D, LEE J W, et al. Electrochemical synthesis of nickel hexacyanoferrate and nickel sulfide on nickel foam as sustainable electrocatalysts for hydrogen generation *via* urea electrolysis[J]. ACS Applied Materials & Interfaces, 2024, 16(50): 69142-69152.

[34] YANG K, HAO L, HOU Y, et al. Summary and application of Ni-based catalysts for electrocatalytic urea oxidation[J]. International Journal of Hydrogen Energy, 2024, 51: 966-981.

[35] ALVAND M, MA Z, KOKATE R, et al. Uncovering the role of vanadium doped Ni_2P for low concentration urea oxidation[J]. Chemical Engineering Journal, 2024, 500: 157130.

[36] CHEN S, ZHANG T, HAN J, et al. Interface engineering of Fe-Sn-Co sulfide/oxyhydroxide heterostructural electrocatalyst for synergistic water splitting[J]. Nano Research Energy, 2024, 3(2): e9120106.

[37] WU T H, LIU Y S, HONG C T, et al. Binary and nanostructured Ni - Mn perovskite fluorides as efficient electrocatalysts for urea oxidation reaction[J]. Journal of Colloid and Interface Science, 2024, 653: 1094-1102.

[38] GUO P, CAO S, HUANG W, et al. Heterojunction-induced rapid transformation of Ni^{3+}/Ni^{2+} sites which mediates urea oxidation for energy-efficient hydrogen production[J]. Advanced Materials, 2024, 36(18): 2311766.

[39] MA D, JIA Y, LI Y, et al. Anion modulate the morphological and electronic structure of NiFe-based electrocatalyst for efficient urea oxidation-assisted water electrolysis[J]. Journal of Materials Science & Technology, 2024, 197: 207-214.

[40] HUANG Z, OU G, XIE Y, et al. NiS - NiS_2 heterostructure for efficient electrocatalytic overall urea splitting [J]. International Journal of Hydrogen Energy, 2024, 49: 1079-1085.

[41] LI H, PU Y, LI W, et al. Sulfur-vacancy engineering accelerates rapid surface reconstruction in Ni-Co bimetal sulfide nanosheet for urea oxidation electrocatalysis[J]. Small, 2024, 20(42): 2403311.

[42] HUANG S, ZHANG Q, XIN P, et al. Construction of Fe-doped NiS - NiS_2 heterostructured microspheres *via* etching Prussian blue analogues for efficient water-urea splitting[J]. Small, 2022, 18(14): 2106841.

[43] ZHENG S L, XU H M, HUANG C J, et al. Regulating the electronic states of $NiSe_2$ by Cr-doping to promote formation of active phases for high catalytic performance

of the urea oxidation reaction[J]. Journal of Materials Chemistry A, 2025, 13(20): 14681-14689.

[44] JIA F, ZHANG Y, ZHANG X, et al. Trimetallic Ni-$CuCoN_{0.6}$ Ohmic junction for the enhanced oxidation of methanol and urea[J]. Journal of Colloid and Interface Science, 2025, 677: 597-607.

[45] WU S, ZHANG Y, ZHANG X, et al. Binary Ni/NiO-$NiWO_4$ with highly activity and durability for the enhanced oxidation of urea[J]. International Journal of Hydrogen Energy, 2024, 85: 261-269.

[46] SHA L, YE K, YIN J, et al. *In situ* grown 3D hierarchical $MnCo_2O_{4.5}$@$Ni(OH)_2$ nanosheet arrays on Ni foam for efficient electrocatalytic urea oxidation[J]. Chemical Engineering Journal, 2020, 381: 122603.

[47] CHENG X, NIE S, HUANG Y, et al. Electron-delocalization across high surface entropy sub-1 nm nanobelts toward enhanced electrocatalytic urea oxidation [J]. Small, 2024, 20(44): 2404595.

[48] HUANG K, QI H, ZENG W, et al. Charge equalization strategy for regulating key intermediate adsorption on bifunctional FeCr-Ni_3S_2 to Boost seawater splitting[J]. Separation and Purification Technology, 2025, 364: 132364.

[49] LINGHU J, GUO R, ZHANG Y, et al. Enhanced methanol oxidation activity of porous layered Ni/CeO_2@CN nanocomposites in alkaline medium [J]. Applied Surface Science, 2023, 631: 157499.

[50] SONG Y, TANG C, HUANG J, et al. Unveiling the promotion of sulfides heterostructure on the urea oxidation reaction: Role of interface engineering and sulfate adsorption[J]. Small, 2025, 21(9): 2410987.

[51] XIAO J, WANG Y, LIU J, et al. Hierarchical Ni/Ni_4Mo nanosheets array on carbon fiber as a bifunctional electrocatalyst for urea-oxidation-assisted water splitting [J]. International Journal of Hydrogen Energy, 2024, 51: 982-992.

[52] JIN L, JI R, WAN H, et al. Boosting the electrocatalytic urea oxidation performance by amorphous - crystalline Ni-TPA@NiSe heterostructures and mechanism discovery [J]. ACS Catalysis, 2023, 13(1): 837-847.

[53] DUAN F, HU Y, LIN J, et al. Construction of CeO_2/Co $(OH)_2$/FeS@NF nanosheet arrays for high-performance electrocatalytic oxygen evolution/urea oxidation, and overall water/urea splitting reactions[J]. International Journal of Hydrogen Energy, 2024, 94: 706-715.

[54] BOCKRIS J O, OTAGAWA T. Mechanism of oxygen evolution on perovskites[J]. The Journal of Physical Chemistry, 1983, 87(15): 2960-2971.

[55] ZHAO H, LIU M, DU X, et al. Construction of nickel stannum based sulfide as efficient electrocatalysts for freshwater, seawater and urea oxidation[J]. International Journal of Hydrogen Energy, 2024, 58: 117-127.

[56] ZHOU S, LV S, SHI J, et al. Self-supported ultrathin NiMn-LDH nanosheets for highly active and robust urea oxidation[J]. Chemical Engineering Journal, 2024, 484: 149706.

[57] DU M, JI Y, LI Y, et al. Construction of an internal charge field: $CoS_{1.097}$/Ni_3S_2 heterojunction promotes efficient urea oxidation reaction[J]. Advanced Functional Materials, 2024, 34(38): 2402776.

[58] CHEN Q, DENG X, HE H, et al. Modulating nanostructure and electronic structure of P and W Co-doped carbon encapsulated heterovalent NiCo composite for accelerating urea oxidation reaction[J]. Chemical Engineering Journal, 2024, 484: 149561.

[59] QIAO G, WANG B, ZHAO Z, et al. Three-dimensional porphyrin and phthalocyanine-based covalent organic frameworks for boosting urea oxidation [J]. Angewandte Chemie International Edition, 2025, 64 (34): e202508783.

[60] WANG T, MIAO L, ZHENG S, et al. Interfacial engineering of Ni_3N/Mo_2N heterojunctions for urea-assisted hydrogen evolution reaction[J]. ACS Catalysis, 2023, 13(7): 4091-4100.

[61] XU S, JIAO D, RUAN X, et al. O-2p hybridization enhanced transformation of active γ-NiOOH by chromium doping for efficient urea oxidation reaction[J]. Advanced Functional Materials, 2024, 34(36): 2401265.

[62] ZHAO X. Superior electrocatalytic performance of nitrogen-doped carbon-embedded Ni/NiO/NiB nanocrystals for urea oxidation[J]. New Journal of Chemistry, 2024, 48(44): 18900-18907.

[63] WU N, CHI X, ZHANG Y, et al. Convenient synthesis and enhanced urea oxidation of NiO - CrO@N - C[J]. New Journal of Chemistry, 2024, 48(13): 5621-5626.

[64] LI C, ZHANG Y. Cr-doped NiO nanocrystals anchored on wood-based carbon for enhanced electrocatalytic oxidation of urea[J]. International Journal of Electrochemical Science, 2024, 19(11): 100805.